

LETTER TO THE EDITOR

Radial and vertical dust transport inhibit refractory carbon depletion in protoplanetary disks

L. Klarmann, C. W. Ormel, and C. Dominik

Astronomical Institute Anton Pannekoek, University of Amsterdam, Science Park 904, 1098 XH Amsterdam, The Netherlands
e-mail: l.a.klarmann@uva.nl

Received 26 June 2018 / Accepted 5 September 2018

ABSTRACT

Context. The Earth is strongly depleted in carbon compared to the dust in the ISM, implying efficient removal of refractory carbon before parent body formation. It has been argued that grains get rid of their carbon through oxidation and photolysis in the exposed upper disk layers.

Aims. We assess the efficacy of these C-removal mechanisms, while accounting for the vertical and radial transport of grains.

Methods. We obtained the carbon and carbon free mass budget of solids by solving two 1D advection-diffusion equations, accounting for the dust grain size distribution and radial transport. The carbon removal acts on the fraction of the grains that are in the exposed layer and requires efficient vertical transport.

Results. In models without radial transport, oxidation and photolysis can destroy most of the refractory carbon in terrestrial planet formation region. But it only reaches the observed depletion levels for extreme parameter combinations and requires that parent body formation was delayed by 1 Myr. Adding radial transport of solids prevents the depletion entirely, leaving refractory carbon equally distributed throughout the disk.

Conclusions. It is unlikely that the observed carbon depletion can ultimately be attributed to mechanisms operating on small grains in the disk surface layers. Other mechanisms of removing carbon quickly and deeply must be studied, for example flash heating events or FU Ori outbursts. However, a sustained drift barrier or strongly reduced radial grain mobility is necessary to prevent replenishment of carbon from the outer disk.

Key words. protoplanetary disks – planets and satellites: composition – astrochemistry

1. Introduction

The Earth is significantly depleted in carbon (Allègre et al. 2001). Its silicon to carbon ratio is a factor of 10^{-4} lower than in the Sun (Grevesse et al. 2010) or in the interstellar medium (ISM), the base material it formed from Bergin et al. (2015). The picture is different for objects formed further out in the solar nebula. The silicon to carbon ratio of carbonaceous chondrites is only a factor 100 lower than in the ISM (Wasson & Kallemeyn 1988), and many comets are not carbon depleted at all (Wooden 2008). This seems to show a gradient of carbon depletion in the solar system, with depletion getting stronger for objects that formed closer to the Sun (e.g. Pontoppidan et al. 2014; Lee et al. 2010; Geiss 1987).

However, more than half of the carbon in the ISM is expected to be refractory material (Zubko et al. 2004). Several processes have been suggested to remove this refractory carbon from the inner regions of a protoplanetary disks. Gail & Trieloff (2017) investigate the destruction of refractory carbon species within their radial transport models (see also Gail 2001), but find that oxidation in the disk mid-plane via OH molecules (Finocchi et al. 1997) is not sufficient to deplete the inner disk region of carbon. Anderson et al. (2017) employ carbon oxidation via atomic oxygen in the hot, upper disk layer (following Lee et al. 2010) and the photolysis of carbon grains directly via UV photons (Alata et al. 2014). In the inner disk

regions they reach a carbon depletion comparable to the Earth, but only if all refractory material is in small grains and without taking into account radial dust transport. In this work, we study how the presence of large grains and vertical and radial dust transport influence the refractory carbon in a protoplanetary disk. We investigate the viability of depleting the inner disk region via oxidation and photolysis in the upper disk layers.

2. Model

2.1. Disk model

For the star we took $M_{\star} = 1 M_{\odot}$, $L_{\star} = 1 L_{\odot}$ and the UV field was set to $L_{UV} = 0.01 L_{\star}$. The total disk mass is set to $0.039 M_{\odot}$. We adopted a dust-to-gas ratio of 0.01, similar to Anderson et al. (2017) and Kamp et al. (2017). The disk surface density follows a power-law profile with $\Sigma \propto r^{-1}$ and is exponentially cut-off at 200 au. The carbon mass fraction $f_c(r)$ is defined as the ratio of the solid carbon surface density and the total dust surface density, $f_c = \Sigma_c / \Sigma_{tot}$. We assumed an initial carbon-to-hydrogen abundance of 2×10^{-4} , which agrees with solar (Asplund et al. 2009) and ISM abundances (Jenkins 2009). Like Anderson et al. (2017), we divided carbon equally between volatiles and refractory grains (see also Zubko et al. 2004). This leads to an initial refractory carbon mass fraction of $f_c \approx 0.25$.

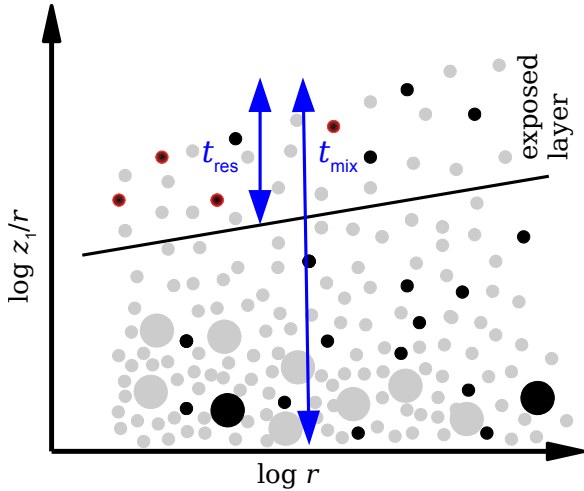


Fig. 1. Height of the exposed layer divided by the disk radius z_1/r against disk radius r . Silicate grains are plotted in grey, carbon grains in black. Large grains are settled close to the midplane. In the exposed layer above z_1 , carbon grains can be oxidised, indicated in red. The range of vertical dust movement is shown by blue arrows. Grains stay for t_{res} in the exposed layer, and within t_{mix} , material from the exposed layer is well-mixed with material from the midplane.

We used a 1+1 D approach to describe the dust movement and composition. The radial dust transport, together with grain growth and fragmentation, is modelled using the *twopoppy* code by Birnstiel et al. (2012, 2015) and using a fragmentation velocity $v_f = 10 \text{ m s}^{-1}$ throughout the disk (see Appendix B).

We refer to the surface layer of the disk where the refractory carbon gets destroyed as the exposed layer, because that layer is exposed to UV photons from the star. This is the layer where carbon reacts with free oxygen and where most of the photolysis occurs. We denote the vertical coordinate of the exposed layer as z_1 and its dust surface density as Σ^* . Figure 1 shows the model setup, depicting the exposed layer above a height z_1 as a function of the disk radius r . It also indicates the vertical range of the dust movement described in Sect. 2.4.

2.2. Calculation of the location of the exposed layer

The exposed layer can be reached by stellar photons. Determining the height z_1 of the exposed layer comes down to determining the height at which small grains still coupled to the gas provide the required optical depth. Because of the flaring geometry of the disk, a radial optical depth $\tau_r = 1$ corresponds to a vertical depth $\tau_z = \Phi$ where $\Phi = 0.05$ is the disk flaring angle. The value of z_1 depends on the total dust surface density Σ_{tot} , the grain size distribution, the grain opacity κ , and grain settling. We assumed that the grains in the exposed layer are in the Rayleigh regime and take $\kappa = \kappa_0 = 2 \times 10^4 \text{ cm}^2 \text{ g}^{-1}$ independent of grain radius s^1 . The surface density Σ^* of the exposed layer then follows, $\Sigma^* = \Phi/\kappa_0$. For simplicity, we assumed that large grains in the optically geometrical limit, $s > s_{\text{geo}} = \lambda/2\pi \approx 0.1 \mu\text{m}$ for $\lambda = 0.55 \mu\text{m}$, do not contribute to the optical opacity. Then,

$$\tau_z(s, z) = f_{\leq s} f_{\geq z} \Sigma^* \kappa_0 \quad (1)$$

¹ We used $\kappa_0 = 2 \times 10^4 \text{ g}^{-1} \text{ cm}^2$, which corresponds to a grain size distribution up to $0.1 \mu\text{m}$ with $f_c = 0.15$ (Min et al. 2016). A correct opacity treatment would take the local grainsize distribution and f_c into account, as well as icy grains in the outer disk. This could change κ_0 by a factor of about five, an effect we explored in a small parameter study.

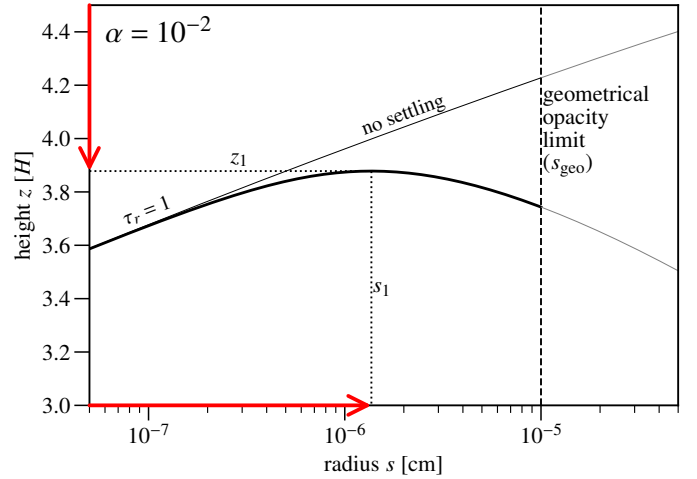


Fig. 2. Height z vs. grain radius s where $\tau_r = 1$ at $r = 1 \text{ au}$. The peak of the z coordinate of τ_r defines the height of the exposed layer z_1 and the radius s_1 up to which grains contribute to the opacity in the exposed layer (red arrows). Grains larger than s_1 are too settled to contribute. The size s_{geo} is an upper limit for s_1 as the opacity decreases with larger grain sizes.

where $f_{\leq s} = (s/s_{\text{max}})^{4-p}$ is the fraction by mass of grains smaller than radius s , assuming a power-law size distribution with exponent with $p = 3.5$ and maximum grain radius s_{max} determined by drift and fragmentation (see Appendix B). Similarly $f_{\geq z}$ is the fraction of the surface density above height z

$$f_{\geq z}(s, z) = \frac{1}{2} \text{erfc} \left(\frac{z}{\sqrt{2} h_{\text{gr}}(s, z)} \right). \quad (2)$$

In calculating this fraction we have used the dust scale height h_{gr} based on the local Stokes number St corresponding to z and the turbulent α parameter, $h_{\text{gr}} = H \sqrt{\alpha / (\alpha + \text{St}(z, s))}$. Hence $f_{\leq s}$ increases with s while $f_{\geq z}$ (for a fixed z) decreases with s .

Figure 2 illustrates these points, plotting the height z where $\tau_r = 1$ as function of grain radius s . Grains contribute to the opacity build up in the exposed layer up to a size s_1 . Ignoring their settling, all grains would contribute to the exposed layer which would therefore lie very high in the disk. In reality settling causes the largest grains to drop out of the exposed layer. We identify the point where $\tau_r = 1$ peaks as the size s_1 and the height z_1 . In our definition of $f_{\geq z}(s, z)$, it is assumed that all grains smaller than s settle to the same height as grains with radius s , which is the reason why $f_{\geq z}(s, z)$ eventually decreases with size s . Although, this would be incorrect in a cumulative sense (extending the distribution to include larger grains should not decrease the mass fraction) it here simply serves the point of finding the size where grains decouple.

2.3. Carbon removal

Carbon removal in the exposed layer occurs via oxidation or photolysis (see Appendix A). The oxidation time for one carbon grain in the exposed layer is

$$t_{\text{ox}} = \frac{4}{3} \frac{s_1 \rho_c}{n_{\text{ox}} v_{\text{ox}} Y_{\text{ox}} m_c} \quad (3)$$

where $\rho_c = 2 \text{ g cm}^{-3}$ is the specific density of the carbon grain material, m_c the mass of a carbon atom, n_{ox} the number density

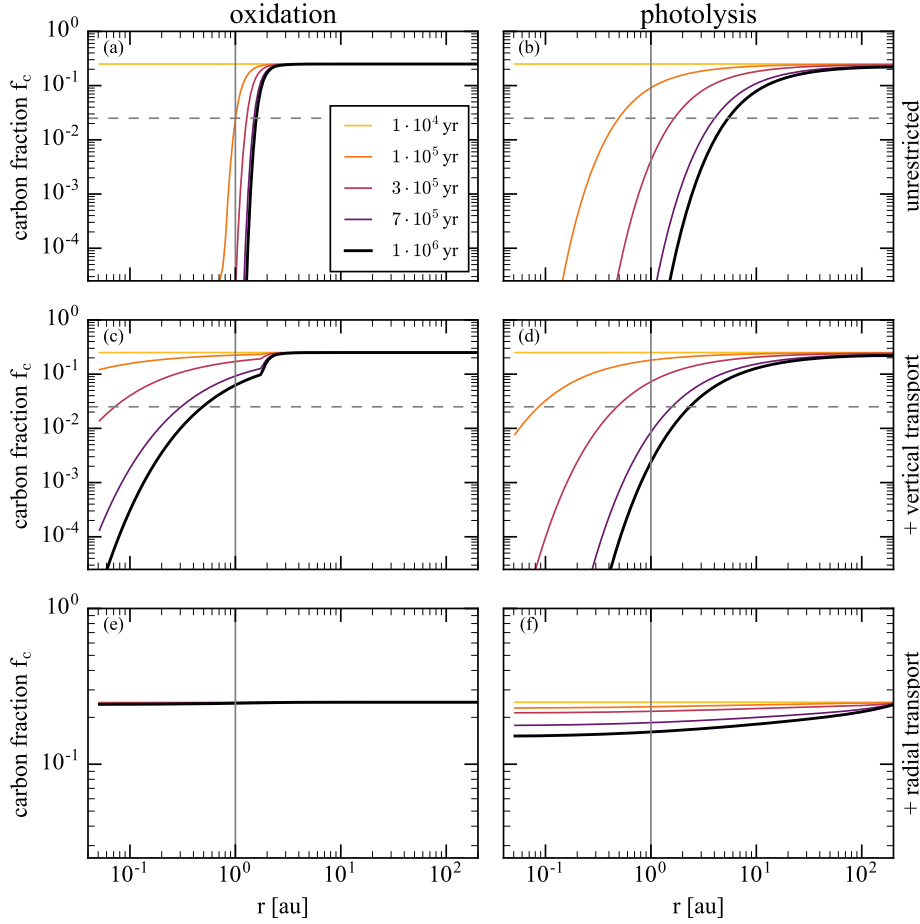


Fig. 3. All panels show the carbon fraction $f_c = \Sigma_c/\Sigma_{\text{tot}}$ as function of disk radius r . Coloured lines show the time evolution of the carbon fraction f_c in the fiducial model from 10^4 yr to 10^6 yr. The vertical line indicates Earth's position. The horizontal dashed line shows depletion by a factor ten. *Left:* carbon removal by oxidation. *Right:* carbon removal by photolysis. *Top panels:* the oxidation (photolysis) $f_c \Sigma^*/t_{\text{ox}}$ ($f_c \Sigma_{\text{ph}}^*/t_{\text{ph}}$) is applied to the carbon in the exposed layer unrestricted by vertical or radial transport. *Middle panels:* vertical dust transport is taken into account as described in Eq. (7) (Eq. (A.9)). *Bottom panels:* vertical and radial dust transport as described in Appendix B are included. The scale of the y-axis has been changed because of the low level of carbon depletion in these models.

of oxygen atoms at z_1 , v_{ox} the oxygen thermal velocity and Y_{ox} the yield of the oxidation (Draine 1979). The photolysis rate is

$$\frac{d\Sigma_c}{dt} = \Phi F_{\text{UV}} Y_{\text{ph}} m_c f_c, \quad (4)$$

where F_{UV} is the UV flux and m_c the mass of a carbon atom. The flaring angle Φ corrects for the fact that the UV photons do not hit the disk surface perpendicular. The yield is $Y_{\text{ph}} = 8 \times 10^{-4}$ (Alata et al. 2014, 2015).

A more detailed description of these processes can be found in Lee et al. (2010) and Anderson et al. (2017) and in Appendix A.

2.4. Effects of vertical dust transport on removal rates

The efficacy of carbon removal is limited by the ability to vertical transport (cycle) the dust. There are two important timescales regarding to the vertical motions of grains. The first is the overall mixing time t_{mix} , indicating on what timescale material from the midplane and the exposed layer become well-mixed. We obtain t_{mix} from the turbulent diffusivity and the gas scale height H :

$$t_{\text{mix}} = \frac{H^2}{\nu_t} = \frac{1}{\Omega \alpha} = 100 \text{ yr} \left(\frac{\alpha}{10^{-2}} \right)^{-1} \left(\frac{r}{\text{au}} \right)^{3/2} \quad (5)$$

where the turbulent diffusivity is assumed equal to the gas viscosity ν_t and is parametrised using the α prescription ($\nu_t = \alpha H^2 \Omega$; Shakura & Sunyaev 1973) with Ω the Keplerian frequency. After one mixing timescale, carbon-depleted material from the exposed layer and carbon-rich material from the midplane are well mixed.

The other relevant timescale is the residence time² of a grain in the exposed layer

$$t_{\text{res}} = \left(\frac{H}{z_1} \right)^2 \frac{1}{\Omega \alpha} = 11 \text{ yr} \left(\frac{z_1}{3H} \right)^{-2} \left(\frac{\alpha}{10^{-2}} \right)^{-1} \left(\frac{r}{\text{au}} \right)^{3/2}. \quad (6)$$

This time is shorter than t_{mix} because the local pressure scale height at height $z \gg H$ is given by H^2/z . A long t_{res} would limit carbon destruction, because the exposed layer will become depleted in refractory carbon. In that case no carbon will be burned, because carbon-free solids build up the opacity in the exposed layer. Hence, carbon removal becomes inefficient when t_{res} is longer than the time to burn a single grain t_{ox} (see Eq. (3)).

Accounting for these vertical transport effects, we obtain a carbon destruction rate of:

$$\frac{d\Sigma_c}{dt} = 2f_c \cdot \min \left(\frac{\Sigma^*}{t_{\text{ox}}}, \frac{\Sigma^*}{t_{\text{res}}}, \frac{f_{\leq s_1} \Sigma_{\text{tot}}}{t_{\text{mix}}} \right) \quad (7)$$

where the factor two accounts for the two sides of the disk and Σ_c is the surface density of carbon grains with $s < s_1$. This expression applies to C-burning; in Appendix A.2 a similar expression is derived for photolysis.

3. Results

Our results are presented in Fig. 3 for the oxidation (left) and the photolysis (right) models.

² Anderson et al. (2017) define t_{res} differently, as the total time a grain spends in the exposed layer over 1 Myr.

Table 1. Carbon fraction $f_c = \Sigma_c/\Sigma_{\text{tot}}$ after 1 Myr at 1 au for models limited by vertical transport and models limited by vertical and radial transport.

Variation	Value	f_c at 1 au after 1 Myr	
		only vertical transport	vertical + radial transport
Fiducial		1.7×10^{-3}	0.16
Higher UV-flux	$L_{\text{UV}} = 0.1 L_{\star}$	5.2×10^{-5}	0.11
Lower opacity	$\kappa_0 = 4 \times 10^3 \text{ cm}^2 \text{ g}^{-1}$	6.4×10^{-11}	0.052
Larger opacity	$\kappa_0 = 1 \times 10^5 \text{ cm}^2 \text{ g}^{-1}$	0.10	0.23
Lower turbulence	$\alpha = 10^{-3}$	0.015	0.24
Less small grains	$p = 3$	0.061	0.23
Lower fragmentation velocity	$v_f = 3 \text{ m s}^{-1}$	4.0×10^{-8}	0.12

Notes. Initial carbon fraction is $f_c = 0.25$. Only one parameter is varied with respect to the fiducial model.

3.1. Unrestricted models

The upper row plots present the carbon fraction f_c without including any transport-limiting factors, in other words, by using only the first term in Eq. (7) ($f_c \Sigma^*/t_{\text{ox}}$). As can be seen, oxidation depletes carbon by a factor of 10^{-4} out to 1.1 au. Beyond this point carbon burning is essentially shut off, because of the exponential dependence of the oxidation yield Y_{ox} on temperature. The photolysis rate, on the other hand, does not depend on temperature ($F_{\text{UV}} \propto r^{-2}$ but Y_{ph} is constant). After 1 Myr, the disk is depleted by a factor of 10^{-4} out to 1.3 au and by a factor of 0.1 out to 7 au.

3.2. Vertical dust transport

Accounting for vertical transport effects – that is, including all three regimes in Eq. (7) – we see that oxidation (Fig. 3c) and photolysis (Fig. 3d) become less effective. Carbon oxidation inward of 1.3 au becomes now limited by the residence time t_{res} . Grains that make it into the exposed layer burn their carbon atoms completely, rendering the overall burning inefficient. Similarly, the photolysis rate equals $f_c \Sigma_{\text{ph}}^*/t_{\text{res-ph}}$ everywhere. The photolysis rate tends to be larger than the oxidation rate, because the UV photons penetrate more deeply, resulting in a larger exposed layer (see Appendix A.2). However, the photolysis run reaches depletion levels just short of 10^{-4} at 1 au.

3.3. Vertical and radial dust transport

Accounting in addition for radial transport (bottom panels of Fig. 3) further reduces the efficacy of carbon destruction. Carbon-rich solids from the outer disk simply drift into the inner region to replenish any carbon depleted material. The carbon destruction becomes drift-limited: carbon will only be depleted when the local destruction time ($t_{\text{destr}} = \Sigma_c/(d\Sigma_c/dt)$) becomes shorter than the drift timescale t_{drift} of the (mass-dominating) pebbles. Since t_{drift} tends to be rather short (200 yr at 1 au) depletion is minimal with little variation throughout the disk.

3.4. Parameter variation

In Table 1 we list the results from additional photolysis runs, quantifying the level of carbon depletion at 1 au after 1 Myr. A higher opacity, a lower α or a shallower grain size distribution ($p = 3$; fewer small grains) only reduce the carbon destruction, because Σ^* becomes lower or t_{res} increases. For the runs without radial transport, a stronger UV field enhances the depletion as the UV photons penetrate deeper. It can be argued that the low

κ_0 run is more appropriate for the opacity in the exposed layer, when the grains lose most of their carbon. This will increase Σ^* , and completely remove all carbon interior to 1 au – but only when there is no radial replenishment. Similarly, reducing the fragmentation velocity to 3 m s^{-1} leads to more small grains and therefore a stronger depletion at 1 au in the case of only vertical transport. When radial transport is included, the carbon fraction is only reduced by a factor of two. Since the fragmentation velocity outside of the snowline is expected to be much higher than 3 m s^{-1} , a more realistic case where the fragmentation velocity depends on the disk radius would lead to even less carbon depletion. In general, the replenishment of carbon via radial transport renders the depletion independent of the adopted parameters.

4. Discussion and conclusion

Our findings regarding unrestricted C-burning are in line with the study of Anderson et al. (2017). They, too, find that photolysis is the more significant C-depletion mechanism and that the inner disk can become devoid in carbon. Like us, Anderson et al. (2017) account for the limited total time grains spend in the exposed layers. However, they have overestimated the removal by incorrectly assuming that each stay in the exposed layer is short enough to ensure a continuous supply of carbon in the exposed layer. Instead, we found (even in the case of high turbulence) that carbon-depleted grains stay longer in the exposed layer than the time it takes to remove their carbon. This makes both oxidation and photolysis inefficient. Furthermore, adding radial dust transport to the model makes it impossible to deplete the inner disk of carbon even under extreme assumptions about the UV field of the early Sun or the grain opacities.

It is unlikely that other C-destruction mechanisms can change this outcome. Adding oxidation of carbon by OH in the midplane does not increase the carbon depletion sufficiently (Gail & Tieloff 2017). For high accretion rates, the midplane region can be heated to roughly 1500 K out to 2 au (Min et al. 2011). However, these accretion rates must then be sustained over a significant time to allow the Earth’s building blocks to form.

Therefore, we conclude that the only way to ensure the C depletion factors as observed in the solar system is to invoke an early hot or intense inner disk environment to ensure rapid C-destruction before parent body formation. This needs to happen in combination with a sustained barrier for drift to prevent C-replenishment, for example by the formation of a giant planet. FU Orionis events can lead to inner disk temperatures of several thousand Kelvin (Hartmann & Kenyon 1996; Zhu et al. 2007) over several decades. The composition of chondrules indicate

that several flash heating events happened in the solar nebula (Ciesla et al. 2005; Jones et al. 2000), reaching temperatures of around 2000 K nearly instantly and cooling again within days. To prevent the fast replenishment of carbon, these events need to happen at a high frequency, comparable to the drift timescale. Events at a lower rate can also cause a sustained refractory carbon depletion in the inner disk region, but this requires radial grain mobility to be strongly reduced or halted.

Acknowledgements. The authors thank the referee for valuable feedback. The authors thank Inga Kamp for sharing her ProDiMo model, Christian Rab for sharing prodimopy, Michiel Min for sharing OpacityTool, and Til Birnstiel for sharing twopoppy. We thank the above-mentioned and Rens Waters and Kaustubh Hakim for helpful discussions and Sebastiaan Krijt for his thoughtful comments on the manuscript. L.K. is supported by a grant from NOVA. C.W.O. acknowledges funding by the Netherlands Organization for Scientific Research (NWO; VIDI project 639.042.422). C.D. acknowledges funding by the NWO, project number 614.001.552.

References

- Alata, I., Cruz-Díaz, G. A., Muñoz Caro, G. M., & Dartois, E. 2014, *A&A*, **569**, A119
- Alata, I., Jallat, A., Gavilan, L., et al. 2015, *A&A*, **584**, A123
- Allègre, C., Manhès, G., & Lewin, É. 2001, *Earth Planet. Sci. Lett.*, **185**, 49
- Anderson, D. E., Bergin, E. A., Blake, G. A., et al. 2017, *ApJ*, **845**, 13
- Asplund, M., Grevesse, N., Sauval, A. J., & Scott, P. 2009, *ARA&A*, **47**, 481
- Bergin, E. A., Blake, G. A., Ciesla, F., Hirschmann, M. M., & Li, J. 2015, *Proc. Nat. Acad. Sci.*, **112**, 8965
- Birnstiel, T., Klahr, H., & Ercolano, B. 2012, *A&A*, **539**, A148
- Birnstiel, T., Andrews, S. M., Pinilla, P., & Kama, M. 2015, *ApJ*, **813**, L14
- Ciesla, F. J. 2005, in *Chondrites and the Protoplanetary Disk*, eds. A. N. Krot, & E. R. D. Scott, *ASP Conf. Ser.*, **341**, 811
- Draine, B. T. 1979, *ApJ*, **230**, 106
- Fedele, D., van Dishoeck, E. F., Kama, M., Bruderer, S., & Hogerheijde, M. R. 2016, *A&A*, **591**, A95
- Finocchi, F., Gail, H. P., & Duschl, W. J. 1997, *A&A*, **325**, 1264
- Gail, H. P. 2001, *A&A*, **378**, 192
- Gail, H.-P., & Trieloff, M. 2017, *A&A*, **606**, A16
- Geiss, J. 1987, *A&A*, **187**, 859
- Grevesse, N., Asplund, M., Sauval, A. J., & Scott, P. 2010, *Ap&SS*, **328**, 179
- Hartmann, L., & Kenyon, S. J. 1996, *ARA&A*, **34**, 207
- Jenkins, E. B. 2009, *ApJ*, **700**, 1299
- Jones, R. H., Lee, T., Connolly, Jr., H. C., Love, S. G., & Shang, H. 2000, *Protostars and Planets IV*, 927
- Kamp, I., Thi, W.-F., Woitke, P., et al. 2017, *A&A*, **607**, A41
- Lee, J.-E., Bergin, E. A., & Nomura, H. 2010, *ApJ*, **710**, L21
- Meijerink, R., Aresu, G., Kamp, I., et al. 2012, *A&A*, **547**, A68
- Min, M., Dullemond, C. P., Kama, M., & Dominik, C. 2011, *Icarus*, **212**, 416
- Min, M., Rab, C., Woitke, P., Dominik, C., & Ménard, F. 2016, *A&A*, **585**, A13
- Pontoppidan, K. M., Salyk, C., & Bergin, E. A., et al. 2014, *Protostars and Planets VI*, 363
- Shakura, N. I., & Sunyaev, R. A. 1973, *A&A*, **24**, 337
- van Zadelhoff, G.-J., Aikawa, Y., Hogerheijde, M. R., & van Dishoeck, E. F. 2003, *A&A*, **397**, 789
- Wasson, J. T., & Kallemeyn, G. W. 1988, *Phil. Trans. R. Soc. London, Ser. A*, **325**, 535
- Wooden, D. H. 2008, *Space Sci. Rev.*, **138**, 75
- Zhu, Z., Hartmann, L., Calvet, N., et al. 2007, *ApJ*, **669**, 483
- Zubko, V., Dwek, E., & Arendt, R. G. 2004, *ApJS*, **152**, 211

Appendix A: Carbon removal

A.1. Oxidation

The exposed layer is characterized by a steep vertical gradient in gas temperature. However, most of the dust in the exposed layer will be found just above z_1 , corresponding to a radial optical depth of unity. Since the penetration of UV photons is also responsible for the heating of the gas, this location can be very well characterized by a single temperature. Based on previous observations and thermo-chemical disk modelling (Fedele et al. 2016; Kamp et al. 2017), we described the gas temperature in the exposed layer by

$$T_g = T_i \left(\frac{r}{r_i} \right)^{-q}, \quad (\text{A.1})$$

with $T_i = 750$ K, $r_i = 1$ au and $q = 0.6$. This temperature leads to a mean thermal velocity of oxygen atoms of

$$v_{\text{ox}} = \sqrt{\frac{8k_B T_g}{\pi m_{\text{ox}}}}, \quad (\text{A.2})$$

where k_B is Boltzmann's constant and m_{ox} is the mass of an oxygen atom.

The gas number density at z_1 is then

$$n_g = \frac{\Sigma_g}{\sqrt{2\pi\mu m_p H}} \exp\left(-\frac{z_1^2}{2H^2}\right), \quad (\text{A.3})$$

where Σ_g is the gas surface density, $\mu = 2.35$ the mean molecular weight and m_p the proton mass. We used the oxygen number density at z_1 , $n_{\text{ox}} = \epsilon n_g$, with $\epsilon = 10^{-4}$ as found in ProDiMo models by Meijerink et al. (2012) and similar to the value of $\epsilon \approx 2 \times 10^{-4}$ shown in Lee et al. (2010).

The probability of removing a carbon atom when a carbon grain is hit by an oxygen atom is given by the yield

$$Y_{\text{ox}} = A \exp(-B/T_g), \quad (\text{A.4})$$

with $A = 2.3$, $B = 2580$ for $T_g < 440$ K and $A = 170$, $B = 4430$ for $T_g > 440$ K (Draine 1979).

The rate at which carbon is removed from a single grain by oxidation is

$$k_{\text{ox}} = n_{\text{ox}} v_{\text{ox}} \sigma Y_{\text{ox}}, \quad (\text{A.5})$$

where $\sigma = \pi s^2$ is the grain cross section. For grains with radius s_1 this leads to a carbon destruction time of:

$$t_{\text{ox}} = \frac{m_{\text{gr}}}{m_c k_{\text{ox}}} = \frac{4}{3} \frac{s_1 \rho_c}{n_{\text{ox}} v_{\text{ox}} Y_{\text{ox}} m_c} \quad (\text{A.6})$$

with m_{gr} the mass of a carbon grain. Grains lose all their carbon when they reside for a time $t \gg t_{\text{ox}}$ in the exposed layer. The change in grain radius during oxidation is not taken into account in our model.

A.2. Photolysis

In the case of photolysis by UV photons, a fraction $f_c Y_{\text{ph}}$ of the absorbed photons will remove a carbon atom directly, resulting in a destruction rate of

$$\left(\frac{d\Sigma_c}{dt} \right)_{\text{ph-unrestricted}} = \Phi F_{\text{UV}} Y_{\text{ph}} m_c f_c \quad (\text{A.7})$$

where F_{UV} is the UV field. The flaring angle Φ corrects for the fact that the UV photons do not hit the disk surface perpendicular. The yield is $Y_{\text{ph}} = 8 \times 10^{-4}$ (Alata et al. 2014, 2015; Anderson et al. 2017).

Analogous to oxidation, photolysis can also be limited by the residence timescale. However, in the case of photolysis UV photons can reach disk layers below the optical $\tau_r = 1$ line, due to forward scattering into the disk (van Zadelhoff et al. 2003). We calculated the height z_1 of the layer exposed to UV radiation by equating t_{res} , the residence time, with t_{ph} , the time to destroy a carbon grain entirely by photolysis:

$$\left(\frac{H}{z_1} \right)^2 \frac{1}{\Omega \alpha} = \frac{4}{3} \frac{s_1 \rho_c}{F_{\text{UV}} Y_{\text{ph}} m_c} \exp(\tau_r(s_1, z_1)). \quad (\text{A.8})$$

Here, the exponential factor expresses the attenuation of the UV field within the disk. Analogous to the $\tau_r = 1$ constraint for the oxidation case, we use this equation to find the height of the exposed layer $z_{1,\text{ph}}$, the value of the optical depth at $z_{1,\text{ph}}$, $\tau_{r,\text{ph}}$ (now generally larger than unity) and the amount of exposed material $\Sigma_{\text{ph}}^* = \tau_{r,\text{ph}} \Phi / \kappa$. Once the layer that is exposed to photolysis is thus characterised, the carbon destruction is calculated using the rates as shown in Eq. (7). Using Eq. (A.7) for the unrestricted photolysis rate, the carbon removal rate then becomes

$$\left(\frac{d\Sigma_c}{dt} \right)_{\text{ph}} = 2f_c \cdot \min\left(\frac{\Sigma_{\text{ph}}^*}{t_{\text{ph}}}, \frac{\Sigma_{\text{ph}}^*}{t_{\text{res-ph}}}, \frac{f_{\leq s_1} \Sigma_{\text{tot}}}{t_{\text{mix}}} \right) \quad (\text{A.9})$$

where $t_{\text{res-ph}}$ now follows from the solution to Eq. (A.8).

Appendix B: Radial dust transport

We used the twopopy code by Birnstiel et al. (2012, 2015) to model the radial movement of dust grains. In this code, the dust mass is assigned to two grain sizes: small and large. The small grain radius is chosen so that the grains are well coupled to the gas. The radius of the large grains (as well as the ratio of the mass distribution) depends on the local disk conditions, is limited (mainly) by drift and fragmentation and is updated after each timestep. This makes it possible to describe the dust evolution of the disk based on two surface densities. We give here only a short overview over the most important concepts and formulas.

Assuming that the Epstein limit of the drag law applies to all relevant grain sizes in the entire disk, compact spherical grains, a self-similar gas surface density profile and an eddy turn over time of $t_L = 1/\Omega$, the Stokes number St_{mid} of a grain with radius s and specific density ρ_s at the midplane can be written as

$$\text{St}_{\text{mid}} = \frac{s \rho_s \pi}{\Sigma_g} \frac{\pi}{2}. \quad (\text{B.1})$$

The small, well-coupled grains have a fixed radius, which we assume to be $s_s = 0.1 \mu\text{m}$. The size of the large grains is limited by fragmentation and drift. The size limit due to fragmentation is given by

$$s_{\text{frag}} = f_f \frac{2}{3\pi} \frac{\Sigma_g}{\rho_s \alpha} \frac{v_f^2}{c_s^2}, \quad (\text{B.2})$$

where c_s is the isothermal sound speed and f_f is a calibration factor of order unity, leading to grain size slightly below the fragmentation limit. The size limit due to drift is given by

$$s_{\text{drift}} = f_d \frac{2}{\pi} \frac{\Sigma_d}{\rho_s} \frac{(\Omega r)^2}{c_s^2} \left| \frac{d \ln P}{d \ln r} \right|^{-1}, \quad (\text{B.3})$$

where P is the gas pressure and f_d is a calibration factor similar to f_f . The radius of the large grains is then chosen as $s_1 = \min(s_{\text{drift}}, s_{\text{frag}})$.

In the fragmentation limited regime, the surface density fraction in large grains is $f_l = 0.75$, and $f_l = 0.97$ in the drift limited regime. We emphasise that these mass distributions and grain sizes are used for the radial and not the vertical dust transport. Only the maximum possible grain size $s_{\text{max}} = s_1$ is used in the calculation of s_1 and z_1 in Sect. 2.2.

The radial transport of the dust can now be described by solving two advection-diffusion equations:

$$\frac{\partial \Sigma_i}{\partial t} + \frac{1}{r} \frac{\partial}{\partial r} \left[r \left(\Sigma_i v_i - D_i \Sigma_g \frac{\partial}{\partial r} \left(\frac{\Sigma_i}{\Sigma_g} \right) \right) \right] = 0 \quad (\text{B.4})$$

where Σ_i is the surface density of the dust grain, v_i the dust velocity due to drift and gas drag, D_i the diffusivity of the species and the index i refers to the small (s) and the large (l) grains. For the small dust component v_i will be equal to the gas accretion velocity while for the large component the drift velocity and the gas accretion velocity both contribute. Since the Stokes number of a grain is always smaller than unity in this model, the dust diffusivity is assumed to be equal to the gas diffusivity D_g which is considered the same as the gas viscosity.

To follow not only the dust mass and size but also the dust composition, we have modified this code. We used four instead of two types of grains, small and large carbon grains ($s_{c,s}$, $s_{c,l}$) and small and large silicate grains ($s_{s,s}$, $s_{s,l}$). As in the original code, f_i is used to distribute the surface density between the particles sizes, and we use f_c to distribute the surface density between the different grain species. The advection-diffusion equation for small carbon grains now includes a sink term and reads:

$$\frac{\partial \Sigma_{c,s}}{\partial t} + \frac{1}{r} \frac{\partial}{\partial r} \left[r \left(\Sigma_{c,s} v_s - D_s \Sigma_g \frac{\partial}{\partial r} \left(\frac{\Sigma_{c,s}}{\Sigma_g} \right) \right) \right] = - \frac{d \Sigma_c}{dt}. \quad (\text{B.5})$$

The advection-diffusion equation for large carbon grains has no sink term:

$$\frac{\partial \Sigma_{c,l}}{\partial t} + \frac{1}{r} \frac{\partial}{\partial r} \left[r \left(\Sigma_{c,l} v_l - D_l \Sigma_g \frac{\partial}{\partial r} \left(\frac{\Sigma_{c,l}}{\Sigma_g} \right) \right) \right] = 0. \quad (\text{B.6})$$

As in the case of large carbon grains, the advection-diffusion equations for small as well as large silicate grains do not include a sink term.

Once the advection-diffusion equation has been solved, f_c is again calculated, since the radial transport of large and small grains changes the carbon distribution within the disk. By recalculating a new common carbon fraction for both grain sizes after each timestep, we assume that coagulation and fragmentation have been efficient enough to re-distribute carbon between large and small grains. This maximises the carbon removal efficiency. This carbon fraction value is now the base for the calculation of the carbon destruction. When used in Eqs. (7) and (A.9), it does not indicate the carbon fraction in the exposed layer, but is used to calculate the total amount of carbon available in the exposed layer at the onset of oxidation or photolysis.

Through all these calculations, we assumed a constant, self-similar gas surface density profile. The surface density of the destroyed carbon is not added to the gas surface density, but completely removed from the system.

Table B.1. List of notations.

Symbol	Description
Φ	Disk flaring angle
Σ_c	Surface density in carbon grains
$\Sigma_{c,l}$	Surface density of large carbon grains
$\Sigma_{c,s}$	Surface density of small carbon grains
Σ_{tot}	Total dust surface density
Σ^*	Dust surface density in exposed layer (oxidation)
Σ_{ph}^*	Dust surface density in exposed layer (photolysis)
Ω	Keplerian frequency
α	Turbulence parameter
ϵ	Oxygen to gas ratio at z_1
κ	Grain opacity
κ_0	Fixed grain opacity at z_1
λ	Wavelength
μ	Mean molecular weight of neutral hydrogen
ν_t	Turbulent viscosity
ρ_c	Specific carbon grain density
ρ_d	Disk dust density
ρ_g	Disk gas density
ρ_s	Specific grain density
ρ_{tot}	Total disk grain density
σ	Grain cross section
τ_r	Radial optical depth at $0.55 \mu\text{m}$
$\tau_{r,\text{ph}}$	Radial optical depth at $0.55 \mu\text{m}$ at $z_{1,\text{ph}}$
τ_z	Vertical optical depth at $0.55 \mu\text{m}$
A	Parameter for calculation of Y_{ox}
B	Parameter for calculation of Y_{ox}
D_g	Gas diffusivity
D_i	Diffusivity of species i
D_l	Diffusivity of large grains
D_s	Diffusivity of small grains
F_{UV}	UV flux
H	Disk gas scale height
L^*	Stellar luminosity
L_{UV}	Stellar luminosity in the UV
M_*	Stellar mass
P	Gas pressure
T_g	Gas temperature at z_1
T_i	Gas temperature at z_1 at 1 au
St	Stokes number
St_{mid}	Stokes number in midplane
Y_{ox}	Oxidation yield at z_1
Y_{ph}	Photolysis yield
c_s	Isothermal sound speed
f_c	Carbon mass fraction in solids
f_d	Calibration factor for drift limit
f_f	Calibration factor for fragmentation limit
f_l	Surface density fraction of large grains
$f_{\leq s}$	Mass fraction of grains with radius up to s
$f_{\leq s_1}$	Mass fraction of grains with radius up to s_1
$f_{\geq z}$	Fraction of total surface density above z
k_B	Boltzmann's constant
h_{gr}	Dust scale height
k_{ox}	Carbon oxidation rate at z_1
m_{gr}	Mass of grain with s_1
m_c	Mass of a carbon atom
m_{ox}	Mass of an oxygen atom
n_g	Gas number density at z_1

Table B.1. continued.

Symbol	Description
n_{ox}	Oxygen number density at z_1
p	Power law index of grain size distribution
q	Gas temperature power law index at z_1
r	Disk radius
r_i	Reference radius
s	Grain radius
$s_{c,l}$	Radius of large carbon grains
$s_{c,s}$	Radius of small carbon grains
s_{drift}	Maximum grain radius due to drift
s_{frag}	Maximum grain radius due to fragmentation
s_{geo}	Transition grain radius from Rayleigh to geometric regime
s_{max}	Maximum grain radius at r
$s_{s,l}$	Radius of large silicate grains
$s_{s,s}$	Radius of small silicate grains
s_1	Maximum grain radius at z_1
t_{destr}	Destruction timescale at r
t_{drift}	Drift timescale at r
t_L	Eddy turn-over time
t_{mix}	Mixing timescale between z_1 and midplane
t_{ox}	Destruction time of carbon grain with s_1 at z_1 due to oxidation
t_{res}	Residence timescale of grain above z_1
$t_{\text{res-ph}}$	Residence timescale of grain above $z_{1,\text{ph}}$
v_i	Radial grain velocity
v_f	Fragmentation velocity
v_{ox}	Oxygen thermal velocity at z_1
z	Disk height coordinate
z_1	Height of the exposed layer (oxidation)
$z_{1,\text{ph}}$	Height of the exposed layer (photolysis)